

Amora: Black-box Adversarial Morphing Attack

Run Wang¹, Felix Juefei-Xu², Xiaofei Xie¹, Lei Ma³, Yihao Huang⁴, and Yang Liu¹

¹ Nanyang Technological University, Singapore

² Alibaba Group, USA

³ Kyushu University, Japan

⁴ East China Normal University, China

Abstract. Nowadays, digital facial content manipulation has become ubiquitous and realistic with the unprecedented success of generative adversarial networks (GANs) in image synthesis. Unfortunately, face recognition (FR) systems suffer from severe security concerns due to facial image manipulations. In this paper, we investigate and introduce a new type of adversarial attack to evade FR systems by manipulating facial content, called **adversarial morphing attack** (a.k.a. Amora). In contrast to adversarial noise attack that perturbs pixel intensity values by adding human-imperceptible noise, our proposed adversarial morphing attack is a semantic attack that perturbs pixels spatially in a coherent manner. To tackle the black-box attack problem, we have devised a simple yet effective joint dictionary learning pipeline to obtain a proprietary optical flow field for each attack. We have quantitatively and qualitatively demonstrated the effectiveness of our adversarial morphing attack at various levels of morphing intensity on two popular FR systems with smiling facial expression manipulations. Both open-set and closed-set experimental results indicate that a novel black-box adversarial attack based on local deformation is possible, which is vastly different from additive noise based attacks. The findings of this work may pave a new research direction towards a more thorough understanding and investigation of image-based adversarial attacks and defenses.

Keywords: Black-box adversarial attack, morphing, face recognition

1 Introduction

Human faces are important biometrics in identity recognition and access control such as security check, mobile payment, and attendance recording, *etc.* Thus, more and more face recognition systems are widely applied in various fields for improving the service qualities and securing crucial assets. In recent years, research has shown that current FR systems are vulnerable to various attacks (*e.g.*, presentation spoofing attack [50] and adversarial noise attack [8]), which bring severe security concerns to the FR systems deployed in security-sensitive applications such as mobile payment. In this work, we investigate that the FR systems are also vulnerable to another new type of adversarial attack, called

adversarial morphing attack, by perturbing pixels spatially in a coherent manner, instead of perturbing pixels by adding imperceptible noise like adversarial noise attack.

Fig. 1 presents three different types of attacks on the FR systems, namely presentation spoofing attack, adversarial noise attack, and our proposed adversarial morphing attack. Presentation spoofing attack is a rather simple attack method by physically presenting a printed paper, wearing eyeglass, *etc.* In contrast to presentation spoofing attack without any pixels perturbation, adversarial noise attack perturbs pixels in images by adding imperceptible noise. Our proposed adversarial morphing attack is a non-additive approach that perturbs pixels spatially in a coherent manner, while adversarial noise attack adds imperceptible noise. Adversarial noise attack is also called adversarial example attack and studies demonstrated that deep neural networks are vulnerable to adversarial examples which are widely found in image [19], texts [17], audio [59], and even malware [20], *etc.* Compared with physical spoofing attack, pixels manipulated by adversarial attack can hardly be detected and poses more severe security concerns than presentation spoofing attack.

Next, we discuss the attack model and present some basic requirements for black-box adversarial attacks. The ultimate goal of the attack is to evade the model by triggering erroneous output and reducing their performance in classification. The basic requirements for adversarial attacks include: (1) The attack should be performed in *black-box* manner. Most of the time, attackers cannot gain any knowledge of the model including model architecture, parameters, and training data, *etc.* (2) The attack should be *transferable*. The crafted examples that attack one target FR system successfully should have high success rate on other FR systems. (3) The attack should be *controllable*. Attackers can control the perturbations in generating adversarial faces and query the successful attack faces in limited times. (4) The crafted attack samples should look *visually realistic* and *semantically sound* to humans. It would be better without any obvious artifacts in the generated adversarial faces.



Fig. 1: Three typical attacks on the FR systems. (a) presentation spoofing attacks (e.g., print attack [14], disguise attack [50], mask attack [36], and replay attack [9]), (b) adversarial noise attack [42,14,19], (c) proposed adversarial morphing attack.

Our adversarial morphing attack satisfies all of the above four requirements. We can effectively attack the FR systems without obtaining any knowledge of the model in a total black-box scenario and the learned attack pattern can be easily transferred to compromising other FR systems. When attacking the FR systems, the adversarial faces are morphed by a learned proprietary morphing field and look visually realistic to the original faces. Fig. 2 illustrates how to morph a face into an adversarial face with proprietary morphing field to tackle

the black-box attack problem. We can also control the intensity of the morphing field to achieve a controllable attack.

Specifically, we first collect numerous frontal and near-frontal faces to attack the FR systems. The successful queries lead to perpetrating faces and flow field pairs, which are used for learning the universal morphing field bases. Then, for any given candidate face during the attack, we assign a proprietary morphing field in each individual attack and morph each and every single face accordingly. The main contributions of our work are summarized as follows:

(1) In this paper, we introduce a novel type of black-box adversarial attack, namely the black-box adversarial morphing attack (a.k.a. Amora), that morphs facial images with learned proprietary morphing field to generate visually realistic faces that are misclassified by widely adopted FR systems. (2) We devise a simple yet effective method based on joint dictionary learning to learn universal morphing field bases and proprietary morphing fields for generating adversarial faces to evade the FR systems. (3) We have demonstrated the effectiveness of our adversarial morphing attack on two popular FR systems (both closed-set and open-set) with smiling facial expression manipulations without obtaining any knowledge of the FR systems, additionally, our learned proprietary morphing fields also outperform two competitive baselines in morphing facial images to attack the FR systems. (4) Our research findings hint a new research direction towards semantic-based adversarial attacks and defenses by transforming images in a coherent and natural way, as opposed to adding incoherent noises like adversarial noise attack.

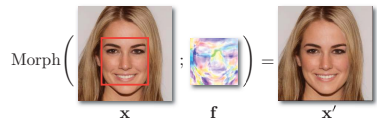


Fig. 2: Adversarial morphing attack with proprietary morphing field. The change is very subtle, and x and x' are indeed different.

2 Related Work

Adversarial Noise Attacks: The FR systems we will be dealing with in this work are all deep learning based ones. It has been demonstrated that, in spite of having achieved very high prediction accuracy, deep neural networks are vulnerable to adversarial attacks [8].

White-box. White-box adversarial attacks require the full knowledge of the deep neural networks. A lot of adversarial attack techniques [19,47,12,43,21,22] have been proposed. These techniques could be applied to attack the face recognition system. Specifically, the fast gradient sign method (FGSM) [18] generates the adversarial examples by performing one step gradient calculation, *i.e.*, adding the sign of gradient of the cost function to the input. Jacobian-based saliency map attack (JSMA) [47] computes the Jacobian matrix which identifies the impact of the input features on the final output, *i.e.*, which pixel has the most significant influence on the change of the output. C&W attack [12] is then proposed to generate adversarial attacks by solving the optimization problem whose basic idea of the objective function is to minimize the perturbation such that the output is changed. DeepFool [43] estimates the closest distance between the input and

the decision boundary. Based on this, the minimal perturbation is calculated for adversarial examples.

Black-box. In a black-box attack setting, the attackers have no way to access model’s parameters or structure and what they can utilize are only input-output pairs. Current techniques which are applied to generate adversarial samples in a black-box setting mainly rely on transferability, gradient estimation, and heuristic algorithms. Papernot *et al.* [46] first exploited the transferability property of adversarial samples to perform a black-box attack. They trained a substitute model based on the input-output relationships of the original model and crafted adversarial samples for the substituted model in a white-box manner. Narodytska *et al.* [44] proposed a local-search method to approximate the network gradients, which was then used to select a small fraction of pixels to perturb. Chen *et al.* [13] utilized the prediction score to estimate the gradients of target model. They applied zeroth-order optimization and stochastic coordinate descent along with various tricks to decrease sample complexity and improve its efficiency. Ilyas *et al.* [25] adopted natural evolutionary strategies to sample the model’s output based on queries around the input and estimate gradient of the model on the input. In addition, noise-based attacks (white/black) may not be realistic, especially in face recognition domain. Differently, our morphing based method can generate a more realistic face which simulates diverse face transformations.

Adversarial Attacks on FR Systems: Sharif *et al.* [50] developed a method to generate attacks, which are realized through printing a pair of eyeglass frames and fool the FR system. Different from the noise-based approach, they adopt the optimization to calculate the perturbation on some restricted pixels (on the glasses frames) and they can be modified by a large amount. Similarly, Bose *et al.* [10] also generate adversarial attacks by solving the optimization constraints based on a generator network. These techniques are white-box attack, which is unrealistic in real-world applications. Additionally, some GAN-based attacking techniques have been proposed. Song *et al.* [51] proposed a GAN, which adds a conditional variational autoencoder and attention modules, for generating fake faces [52,23]. Deb *et al.* [14] proposed AdvFaces that learns to generate minimal perturbations in the salient facial regions via GAN. Dong *et al.* [15] adopted an evolutionary optimization method for generating adversarial samples which is a black-box method. The performance is improved by modeling the local geometry of search directions and reducing the search space. However, they still require many queries. So far there still lacks a work on black-box FR system attack based on pixel morphing that is fully addressed in this work.

Non-additive Adversarial Attacks: The non-additive adversarial attacks have started to gain more attention in the research community. The work of [55] and [7] are the two prior methods that deal with white-box adversarial deformation attacks. In [55], the authors use a second order solver (L-BFGS) to find the deformation vector field, while in [7], a first-order method is formulated to efficiently solve such an optimization. Our method, in contrast, deals with a black-box setting where we cannot have access to the classifier parameters. Therefore, we need to devise a new method to facilitate such an non-additive adversarial

attacks. Wasserstein adversarial attack [54] is also a non-additive attack under the white-box setting that is focused on norm-bounded perturbations based on the Wasserstein distance. The attack covers standard image manipulation such as scaling, rotation, translation, and distortion while our method is able to obtain semantically consistent proprietary morphing field even under a black-box setting. The defense against Wasserstein adversarial attack is also proposed [37]. In this work, we use optical flow as a way to realize facial image morphing and to carry out black-box attacks on the FR systems. It is worth noting that the proposed attack is not on the optical flow estimation step (see [49]), but rather on the face recognition classifier.

Robustness. There are also some techniques proposed for testing the robustness of the model against adversarial examples [60]. DeepXplore [48] proposed the neuron coverage criteria, based which the testing technique is proposed to test multiple deep neural networks (DNNs) as cross-referencing oracles. DeepGauge [40] then proposed a set of more fine-grained testing criteria, such as k -multisection Neuron Coverage, Neuron Boundary Coverage and *etc.* Based on the criteria, a general coverage-guided fuzzing technique, DeepHunter [56], is proposed to test the DNN by maximizing the coverage. In [39], the combinatorial testing criteria are proposed. The surprise metrics [35] are proposed to measure the surprise adequacy of the test set. DeepStellar [16] proposes a set of metrics for RNN testing based on an abstraction of the model. Then the coverage-guided testing technique is developed for testing RNN (*e.g.*, automatic speech recognition). TensorFuzz [45] is another fuzzing framework based on the nearest neighbor metric. In addition, DeepMutation [41] is proposed to evaluate the quality and robustness of the data set (also see [39]) and DiffChaser [57] detects the compatibility issues during the model deployment phase.

3 Proposed Method

Here, we first briefly review the adversarial noise attack and then present an overview of our adversarial morphing attack. Next, we detail how the proposed adversarial morphing attack method learns the universal morphing field bases and obtains a proprietary morphing field for each individual attack.

3.1 Brief Review of Adversarial Noise Attack

In the context of image (gray-scale, RGB, or higher-dimensional) classification problems, let \mathcal{C} be a classifier (shallow or deep) that maps the input image $\mathbf{x} \in \mathbb{R}^N$ to a set of discrete and finite categories $\mathcal{L} = \{1, 2, \dots, L\}$. For simplicity, \mathbf{x} is a vectorized single-channel (gray-scale) image with N pixels in total. *Adversarial noise perturbation attack* aims to find a noise or error vector $\mathbf{e} \in \mathbb{R}^N$ that is small in ℓ_p -norm, *i.e.*, imperceptible, such that when added to the input image can cause erroneous classifier output:

$$\mathcal{C}(\mathbf{x} + \mathbf{e}) \neq \mathcal{C}(\mathbf{x}) \quad \text{and} \quad \|\mathbf{e}\|_p \text{ is small} \quad (1)$$

where $\|\mathbf{e}\|_p = \left(\sum_i^N |e_i|^p\right)^{1/p}$ for $1 \leq p < \infty$ and when $p = \infty$, $\|\mathbf{e}\|_p$ is defined as $\|\mathbf{e}\|_\infty = \max_{i=1, \dots, N} |e_i|$. The search for \mathbf{e} under white-box attack is usually done by back-propagating classifier errors all the way to the noise vector \mathbf{e} . See Sec. 2 for a few popular algorithms. Let $\mathbf{x}' \in \mathbb{R}^N$ be a adversarial noise-perturbed counterpart of \mathbf{x} , the image modification procedure can be summarized as:

$$\mathbf{x}' = \text{Perturb}(\mathbf{x}; \mathbf{e}) = \mathbf{x} + \mathbf{e} \quad (2)$$

Whereas, in this work, we are seeking a non-additive image modification (spatial perturbation of pixels *c.f.* pixel value perturbation) with the aid of optical flow:

$$\mathbf{x}' = \text{Morph}(\mathbf{x}; \mathbf{f}^h, \mathbf{f}^v) \quad (3)$$

where $\mathbf{f}^h \in \mathbb{R}^N$ and $\mathbf{f}^v \in \mathbb{R}^N$ are the horizontal and vertical flow field respectively, and the concatenated whole field is expressed as \mathbf{f} . The actual $\text{Morph}(\cdot)$ function works on 2D images, so there is an implicit step to map the vectorized image and flow fields back to 2D. Modifying images according to Eq. (3) and causing classifier to output erroneously is what we call the *adversarial morphing attack*.

3.2 Overview of Adversarial Morphing Attack

Under the black-box adversarial morphing attack settings, the attackers do not have access to the model parameters (*i.e.*, deep learning based classifier), and thus obtaining the morphing field unique to each attack image by back-propagating the classifier errors through the network parameters is not feasible. In order to obtain proprietary morphing field, we propose to learn a set of universal morphing field bases, and through which, the proprietary morphing field can be reconstructed for each individual attack image. In the next two subsections, we will detail the learning procedure of the universal morphing field bases as well as how to assign a proprietary morphing field.

Fig. 3 outlines the framework of our adversarial morphing attack to learn universal morphing field bases and obtain a proprietary morphing field for each individual attack image. It contains three essential stages: (1) query stage, (2) learning stage, and (3) attacking stage. In the query stage, we collect a set of seed faces and generate morphed faces with GAN to attack the FR systems. Then, in the learning stage, the successful attacks lead to the collection of perpetrating facial images as well as the morphing fields, and from which we will

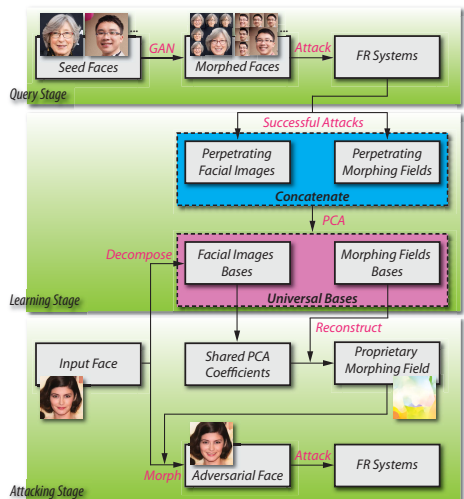


Fig. 3: Overview of the proposed black-box adversarial morphing attack.

learn the universal morphing field bases using joint dictionary learning through principal components analysis (PCA) [53] by concatenating the perpetrating facial images and corresponding perpetrating morphing fields in the learning framework. Finally, in the attacking stage, we obtain a proprietary morphing field for an input face to morph it adversarially for attacking the FR systems.

3.3 Learning Universal Morphing Field Bases

In preparing the training images to learn universal morphing field bases, we first collect numerous frontal and near-frontal faces to generate images with consecutive subtle facial expression change. Specifically, we leverage the power of GAN in digital image manipulation to create a large amount of smiling facial images for each seed face. These morphed smiling facial images are smiled in a controllable way while ensuring other parts relatively unchanged. The consecutive set of smiling faces allows us to accurately capture the morphing field of smiling with optical flow which represents the motion of the pixels between two images. Details are shown in Section 4.

Once we have obtained a large number of (image, morphing field) pairs: $(\mathbf{x}_i, \mathbf{f}_i)$ whose resulting morphed images \mathbf{x}'_i are successful in attacking the model, we can capitalize on the fact that there exists a correlation between the image \mathbf{x}_i and the ‘perpetrating’ morphing field \mathbf{f}_i . There are many ways to learn the 1-to-1 mapping between a given face and its morphing field. Ours draws inspiration from joint dictionary learning for cross-domain generation/matching problems such as super-resolution [58](eq.24 therein), hallucinating full face from periocular region [26](eq.4 therein), *etc.* In this work, we use PCA, a simple yet effective method, to learn the universal morphing field bases. By stacking the corresponding counterparts as part of the same data point, we are implicitly enforcing a 1-to-1 mapping between the two domains (*i.e.*, image and morphing field). Once such a mapping is established between \mathbf{x}_i s and \mathbf{f}_i s, we can potentially reconstruct a proprietary ‘perpetrating’ morphing field for any image of interest. The gist here is to ‘stack’ the two dictionaries (PCA basis for face and morph field) during the optimization process so that they can be learned **jointly** as practiced in [6,27,28,30,31,29]. By doing so, the PCA coefficient vector is ‘forced’ to be shared among the two dictionaries as a ‘bridge’ so that cross-domain reconstruction is made possible. That said, if two sets of PCA bases are learned separately, such projection would not make sense. The training data matrix $\mathbf{X} \in \mathbb{R}^{3N \times M}$ contains concatenated mean-subtracted image and flow field pairs in its columns, with a total of M instances:

$$\mathbf{X} = \begin{bmatrix} \mathbf{A}_x(\mathbf{x}_1 - \boldsymbol{\mu}_x), \dots, \mathbf{A}_x(\mathbf{x}_i - \boldsymbol{\mu}_x), \dots \\ \mathbf{A}_h(\mathbf{f}_1^h - \boldsymbol{\mu}_h), \dots, \mathbf{A}_h(\mathbf{f}_i^h - \boldsymbol{\mu}_h), \dots \\ \mathbf{A}_v(\mathbf{f}_1^v - \boldsymbol{\mu}_v), \dots, \mathbf{A}_v(\mathbf{f}_i^v - \boldsymbol{\mu}_v), \dots \end{bmatrix} \quad (4)$$

where $\mathbf{A}_x \in \mathbb{R}^{N \times N}$, $\mathbf{A}_h \in \mathbb{R}^{N \times N}$, and $\mathbf{A}_v \in \mathbb{R}^{N \times N}$ are diagonal dimensionality weighting matrices for the image, the two flow fields respectively. By setting certain diagonal elements to 0 in \mathbf{A}_x , \mathbf{A}_h , and \mathbf{A}_v , we can arbitrarily select the

region of interest (ROI) in the optimization. In this work, the ROI is tight crop on the face region as shown in Fig. 2 to ignore image deformations outside the face region that may contribute to the successful attacks. However, it might be interesting to explore that in a future work. The bases $\mathbf{w}_i \in \mathbb{R}^{3N}$ can be obtained with the following optimization:

$$J(\mathbf{w}) = \arg \max_{\|\mathbf{w}\|=1} \mathbf{w}^\top \mathbf{X} \mathbf{X}^\top \mathbf{w} = \arg \max_{\|\mathbf{w}\|=1} \frac{\mathbf{w}^\top \mathbf{X} \mathbf{X}^\top \mathbf{w}}{\mathbf{w}^\top \mathbf{w}} = \arg \max_{\|\mathbf{w}\|=1} \frac{\mathbf{w}^\top \mathbf{S}_1 \mathbf{w}}{\mathbf{w}^\top \mathbf{S}_2 \mathbf{w}} \quad (5)$$

where $\mathbf{S}_1 = \mathbf{X} \mathbf{X}^\top$ is the covariance matrix with \mathbf{X} being mean-subtracted, and $\mathbf{S}_2 = \mathbf{I}$. The objective function translates to a generalized Rayleigh quotient and the maximizer \mathbf{w} can be found by solving the eigen-decomposition of $\mathbf{S}_2^{-1} \mathbf{S}_1$ which is $\text{eig}(\mathbf{S}_1)$.

3.4 Assigning Proprietary Morphing Field

For simplicity, let us assume $\mathbf{A}_x = \mathbf{A}_h = \mathbf{A}_v = \mathbf{I}$. The learned universal bases (principal components) can be broken down to an image portion $\mathbf{w}_x \in \mathbb{R}^N$, as well as morphing fields portions $\mathbf{w}_h \in \mathbb{R}^N$ and $\mathbf{w}_v \in \mathbb{R}^N$. When an potential attack image $\mathbf{y} \in \mathbb{R}^N$ comes in, we can decompose it with the top- K , ($K < N$) image portion bases ($\mathbf{W}_x \in \mathbb{R}^{N \times K}$) and obtain the PCA projection coefficient vector $\boldsymbol{\alpha} \in \mathbb{R}^K$:

$$\boldsymbol{\alpha} = (\mathbf{W}_x^\top \mathbf{W}_x)^{-1} \mathbf{W}_x^\top \mathbf{y} \quad (6)$$

By forcing consistent PCA representations during training for both image and flow field, the mapping between the two is implicitly learned. Therefore, we can obtain the proprietary flow field $\mathbf{f}_y \in \mathbb{R}^{2N}$ by reconstructing using the shared coefficients $\boldsymbol{\alpha}$ and the flow field portion $\mathbf{W}_f = [\mathbf{W}_h; \mathbf{W}_v] \in \mathbb{R}^{2N \times K}$ of the bases: $\mathbf{f}_y = \mathbf{W}_f \boldsymbol{\alpha}$. Examples of proprietary morphing fields are shown in Fig. 4.

The first row is the originally given faces and the second row is their proprietary morphing fields learned by our proposed approach.



Fig. 4: Examples of proprietary morphing fields. The first row is the facial images, the second row is the tight cropped faces’ corresponding proprietary optical flow.

4 Experiments

In this section, we present the experimental results to demonstrate the effectiveness of our proposed adversarial morphing attack in evading closed-set and open-set FR systems. We quantitatively and qualitatively evaluate our adversarial morphing attack on two popular FR systems under total black-box scenario. We also demonstrate the transferability of our adversarial morphing attack by investigating whether one adversarial face can be transferred to different FR systems. Additionally, we build several baselines to evaluate whether our learned proprietary morphing field could indeed be effective in evading the FR systems under the ‘imperceptible’ assumption.

4.1 Experimental Settings

Target FR systems. We study two popular FR systems, including VGG-Face [2] with VGG16 and ResNet50 as their architecture. In testing, facial images are morphed by the learned proprietary optical flow field. Then, different intensity level optical flows are calculated to query the successful attack morphing fields. Finally, we use these morphing fields to evaluate the transferability of our attack.

Dataset. We conduct experiments on the CelebFaces Attributes (*CelebA*) [38] and *CelebA-HQ* [33] datasets. *CelebA* contains more than 202,599 face images and 10,177 identities. In training FR systems VGG-Face (VGG16) and VGG-Face (ResNet50) to evaluate the robustness of them in evading our generated morphing facial images, we select 2K and 1K identities from this dataset. *CelebA-HQ* [3] is a high-quality version of the *CelebA* dataset with more than 30K facial images in 1024x1024 resolution. We use this high quality facial images to generate smiling faces with the latest StyleGAN [34,5] to attack the FR systems.

Evaluation metrics. In attacking the FR systems, the morphed facial images should be imperceptible to human eyes and is an adversarial face to the FR systems which leads to misclassification. Thus, some similarity measures between the morphed and the original facial images are needed in order to evaluate the performance of our attack. We will report the mean attack success rate as well as the intensity of the morphing fields. Specifically, we employ the *Euclidean* distance (ℓ_2 -norm) and ℓ_∞ -norm as metrics to measure the intensity of the morphing fields.

Implementation details. Our numerous smiling faces are morphed by StyleGAN and their optical flows are generated using FlowNet2 [24]. StyleGAN utilizes the extended latent space W^+ for editing images with a loss function that is a combination of VGG-16 perceptual loss and pixel-wise MSE loss [4,5], which allows us to generate smiling faces without any visible identity shifts [32] and to capture subtle smiling variations with optical flows. FlowNet2 [1] estimates optical flow between two consecutive images in a learning way. Here, we use FlowNet2 to generate optical flows of facial images which attack the FR systems successfully. All the experiments are performed on a server running Ubuntu 16.04 system on an 18-core 2.30 GHz Xeon CPU with 200 GB RAM and an NVIDIA Tesla M40 GPU with 24 GB memory.

4.2 Experimental Results

Here, we report the experimental results on the *CelebA* dataset. Specifically, we mainly study the following research questions: 1) the effectiveness of the learned proprietary morphing fields in attacking the FR systems, 2) the relation between the attack success rate and intensity of the morphing fields, 3) the transferabilities of our adversarial morphing attack, 4) the capabilities in attacking open-set face recognition systems and 5) the performance in comparing with baselines.

Data preparation. In our experiment, we first collect 182 identities with frontal-face or near frontal-face from *CelebA-HQ* as seed faces to generate morphed smiling faces with StyleGAN. Table 1 presents the number of identities and

facial images in our training dataset, *CelebA-HQ* and *CelebA*. In attacking the FR systems, we randomly select 120 identities including more than 1,000 facial images and morph them with proprietary morphing field to evaluate the robustness of the FR systems against our adversarial morphing attack. Table 2 presents a detailed number of identities and facial images in attacking two popular FR systems. To obtain successfully attacked perpetrating facial images and the pairing morphing fields, we need to attack some FR systems in the query stage. Table 2 presents the number of identities and their corresponding facial images in training the two popular FR systems (*e.g.*, VGG-Face with VGG16 and ResNet50).

Collecting successful attack morphing fields. In the query stage, we generate numerous morphed facial images to attack the FR systems to obtain perpetrating facial images and perpetrating morphing field pairs for learning the universal morphing field bases. Table 3 presents the detailed statistical data of the successful attack pairs. More than 153 and 148 identities from 182 seed faces and nearly 10,000 facial images have successfully attacked the two popular FR systems. In order to obtain large numbers of facial image and morphing field pairs to learn a representative universal morphing field bases, we apply the following strategies to determine a successful attack. 1) causing erroneous output, which directly misclassifies the identity; 2) significant reducing the performance of FR systems, which has low confidence in predicting the identity, *i.e.*, the confidence score is lower than the set threshold $\gamma = 0.6$.

Metrics. Simultaneously, we use a series of metrics to explore the relation between the attack success rate and the intensity of proprietary morphing field. Specifically, we employ two popular metrics ℓ_2 -norm and ℓ_∞ -norm to measure the intensity of proprietary morphing fields.

Adversarial morphing attack. In morphing facial images with learned proprietary morphing fields, we need to identify the range of the intensity of morphing fields and control them to investigate the relation between attack success rate. We first obtain the range of the intensity of morphing fields from the raw morphing fields which have successfully attack the FR systems in the query stage. The intensity of morphing fields are measured with ℓ_2 -norm and ℓ_∞ -norm. To investigate the distribution of the intensity of raw morphing fields, we find that most of the ℓ_2 -norm and ℓ_∞ -norm value lie in a fixed range. Thus, the intensity of proprietary morphing fields is split into several groups according to the fixed range value to evaluate their effectiveness in attacking the target FR systems.

Assigning proprietary morphing fields. Table 4 and Table 5 consolidate the attack success rates vs. different intensity of proprietary optical flow field with ℓ_2 -norm and ℓ_∞ -norm, respectively. The intensity of proprietary morphing fields is mainly split into three groups according to the distribution of the raw morphing fields. In measuring the intensity of proprietary morphing fields with ℓ_2 -norm, the three groups of intensity are as follows: 1) [2, 10] with

Table 1: Identity and images of our collected dataset in the query stage.

	Seed Face	CelebA-HQ	CelebA
id	182	6,217	10,177
img	18,200	30,000	202,599

Table 2: Identities and facial images for attacking and training the 2 popular FR systems.

	Attacking		Training	
	Id	Img	Id	Img
VGG16	120	1,141	2,000	42,256
ResNet50	120	1,159	1,000	21,152

Table 4: Attack success rate with different intensity on proprietary morphing field measured by ℓ_2 -norm.

$\mathcal{M} \setminus \ell_2$	2	4	6	8	10	100	110	120	130	140	150	160	170	180	190	200	300	400	500	600
VGG16	0.34	0.34	0.34	0.34	0.34	0.50	0.48	0.50	0.52	0.57	0.52	0.52	0.55	0.52	0.52	0.52	0.59	0.61	0.61	0.61
ResNet50	0.02	0.02	0.01	0.01	0.01	0.08	0.11	0.10	0.12	0.12	0.12	0.13	0.13	0.14	0.16	0.16	0.23	0.37	0.50	0.60

Table 5: Attack success rate with different intensity on proprietary morphing field measured by ℓ_∞ -norm.

$\mathcal{M} \setminus \ell_\infty$	0.1	0.2	0.3	0.4	0.5	1.0	1.1	1.2	1.3	1.4	1.5	1.6	1.7	1.8	1.9	2.0	3.0	4.0	5.0	6.0
VGG16	0.34	0.34	0.32	0.32	0.34	0.41	0.39	0.46	0.48	0.41	0.48	0.50	0.48	0.50	0.50	0.46	0.55	0.52	0.59	0.55
ResNet50	0.01	0.01	0.01	0.02	0.02	0.04	0.04	0.07	0.06	0.07	0.07	0.07	0.07	0.06	0.07	0.08	0.12	0.18	0.17	0.23

a step value 2; 2) [100, 200] with a step value 10; 3) [200, 600] with a step value 100. In measuring the intensity of proprietary morphing fields with ℓ_∞ -norm, the three groups of intensity are as follows: 1) [0.1, 0.5] with a step value 0.1; 2) [1.0, 2.0] with a step value 0.1; 3) [2.0, 6.0] with a step value 1.0.

Fig. 6 (L) and (C) plot the relation between the attack success rate and the modulated flow field on ℓ_2 -norm and ℓ_∞ -norm. We can find that the success attack is increasing with the intensity of proprietary morphing field. Since the intensity range spans two orders of magnitude, we present the plots in Fig. 6 (L) and (C) in semi-log on the x-axis. Experimental results have shown that VGG-Face with VGG16 as backend architecture is more vulnerable than VGG-Face with ResNet50 as backend architecture. Our Amora can reach and attack success rate at nearly 60% in attacking the two popular FR systems, VGG-Face (VGG16) and VGG-Face (ResNet50). Additionally, we also explore the relation between the attack success rate and the modulated flow field on the multiplier δ for enhancing the intensity of proprietary morphing fields. The range of the coefficient δ is 0.2 to 2.0 with a step value 0.2.

Table 6 presents the results of attack success rate and the intensity of proprietary morphing with multiplier δ . Fig. 6 (R) plots a trend of the increase of the multiplier δ and attack success rate. We can also find that VGG-Face with VGG16 as backend architecture is more vulnerable than VGG-Face with ResNet50 as backend architecture. To get an intuitive visualization of facial images morphed with proprietary morphing fields, we present some morphed facial images of three different identities on the three metrics in Fig. 5.

Table 3: Pair of facial image and morphing fields successfully attack FR systems in the query stage.

	VGG16	ResNet50
Identity	153	148
Morphing Field	9,621	10,536

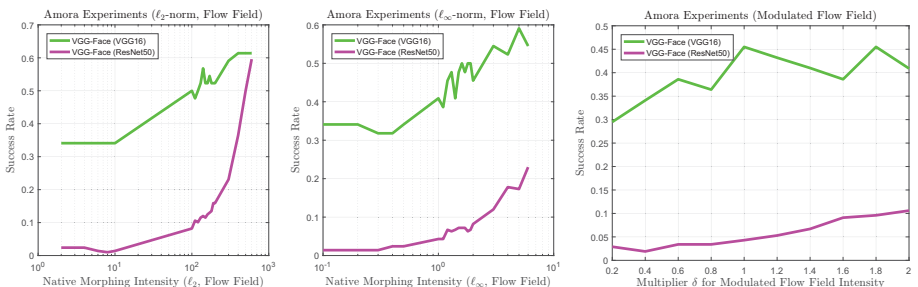
Fig. 6: The relation between the attack success rate and the modulated flow field on ℓ_2 -norm, ℓ_∞ -norm, and multiplier δ .

Table 6: Enhancing the intensity of proprietary morphing fields on the multiplier δ .

$\mathcal{M} \setminus \delta$	0.2	0.4	0.6	0.8	1.0	1.2	1.4	1.6	1.8	2.0
VGG16	0.295	0.341	0.386	0.364	0.455	0.432	0.410	0.386	0.455	0.409
ResNet50	0.029	0.019	0.034	0.034	0.043	0.053	0.067	0.091	0.096	0.106

4.3 Evaluation of Transferabilities

In this section, we mainly discuss the transferabilities of our adversarial morphing attack. Transferability is an important feature in adversarial attack, which means a successful attack in one model could be transferred to other models with high successful attack rate. In our experiment, we demonstrated the effectiveness of our adversarial morphing attack

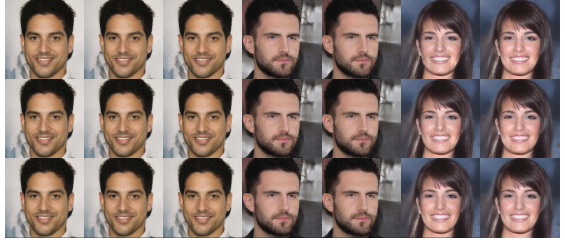


Fig.5: Morphed facial images (IDs from the left to right in *CelebA* are 011141, 003668, and 011910, respectively.) with proprietary morphing fields measured by ℓ_2 -norm (values are 10, 120, 140, 170, 190, 300, 600), ℓ_∞ -norm (values are 0.2, 0.5, 1.0, 1.5, 2.0, 4.0, 6.0), and multiplier δ (values are 0.2, 0.6, 0.8, 1.0, 1.2, 1.4, 2.0), from top to bottom.

by investigating the attack transferabilities between VGG-Face with VGG16 as backend architecture and VGG-Face with ResNet50 as backend architecture. Our transferability evaluation experiments are conducted on a dataset from Table 2. Each facial image is morphed with their proprietary morphing field with ℓ_2 -norm and ℓ_∞ -norm as metrics to control the intensity of morphing field. Table 7 presents us the experimental results in evaluating the transferabilities of adversarial morphing attack. The intensity of proprietary morphing field is measured by ℓ_2 -norm and ℓ_∞ -norm and their value are presented in Table 4 and Table 5, respectively. Experimental results shown that our adversarial morphing attack gives an average 90% success rate in attacking transferabilities evaluation.

4.4 Open-set Evaluation

As open-set face recognition is common, we have evaluated the effectiveness of our approach in attacking closed-set FR systems. In this section, we present the experimental results of our adversarial morphing attack in dealing with open-set attack where the focus is on unseen classes. We trained two popular FR systems with 500 identities on *CelebA-HQ* dataset, namely VGG-Face with VGG16 and ResNet50 as backend. In testing, the identity of a new given face is unseen in training. In the experiment, we evaluate whether our morphed facial images with assigned proprietary morphing fields decrease the performance of open-set FR systems in classification. We use the receiver operating characteristic (ROC) curve to evaluate the performance of our Amora in attacking open-set FR systems. ROC curve is an important and common method for evaluating the performance of classifiers. Verification rate (VR) at 0.001 false accept rate

Table 7: The transferabilities of our proposed adversarial morphing attack between VGG16 and ResNet50 with ℓ_2 -norm and ℓ_∞ -norm.

metrics \ \mathcal{M}	VGG16	ResNet50
ℓ_2 -norm	0.935	0.926
ℓ_∞ -norm	0.893	0.885

Table 8: Open-set face verification scores (verification rate (VR) at 0.001 false accept rate (FAR), equal error rate (EER), and area under the ROC curves (AUC)) with different intensity on proprietary morphing field measured by ℓ_2 -norm on ResNet50 and VGG16 FR systems, respectively.

FR	ℓ_2	2	4	6	8	10	100	110	120	130	140	150	160	170	180	190	200	300	400	500	600	Orig.
ResNet50	VR	93.37	93.33	93.31	93.28	93.26	92.88	92.82	92.53	92.61	92.44	92.28	92.13	91.50	91.44	91.32	90.43	85.19	79.01	71.73	64.49	93.38
	EER	1.52	1.52	1.52	1.52	1.52	1.31	1.30	1.36	1.35	1.42	1.42	1.49	1.47	1.45	1.49	1.52	1.79	2.33	3.13	4.21	1.52
	AUC	99.64	99.64	99.64	99.64	99.64	99.63	99.63	99.64	99.63	99.63	99.62	99.62	99.62	99.62	99.61	99.61	99.58	99.50	99.36	99.18	99.64
VGG16	VR	94.33	94.34	94.40	94.38	94.36	94.71	94.74	94.76	94.80	94.78	94.83	94.80	94.73	94.73	94.64	94.66	93.71	91.83	87.52	82.66	94.69
	EER	1.48	1.46	1.47	1.44	1.44	1.48	1.49	1.55	1.54	1.54	1.58	1.59	1.60	1.59	1.63	1.66	1.70	1.80	2.13	2.73	1.42
	AUC	99.64	99.64	99.64	99.64	99.65	99.68	99.68	99.69	99.69	99.69	99.69	99.69	99.69	99.69	99.69	99.69	99.69	99.71	99.70	99.66	99.56

(FAR), equal error rate (EER), and area under the ROC curve (AUC) are adopted as verification scores for evaluating the performance of our adversarial morphing attack in attacking open-set FR systems. Higher EER means higher attack success rate while lower VR and AUC mean higher attack success rate.

Table 8 presents us the open-set face verification scores with 20 different intensities on proprietary morphing field measured by ℓ_2 -norm on ResNet50 and VGG16 face recognition systems, respectively. The two popular face recognition systems are more easily attacked when the intensity of proprietary morphing fields increased according to the face verification scores VR, EER, and AUC. Fig. 7 shows the ROC curves for the open-set experiments on the ResNet50 and VGG16 face recognition systems, respectively. In Fig. 7, we select six different intensities on the proprietary morphing field measured by ℓ_2 -norm to generate morphed facial images for attacking ResNet50 and VGG16 face recognition systems. The lower AUC means that the face recognition system is more easily attacked. In comparing with the original facial images, we find that our morphed facial images on different intensity proprietary morphing fields can achieve higher possibility in attacking open-set FR systems.

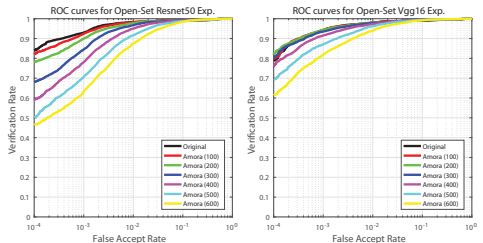


Fig. 7: ROC curves for the open-set experiments on the ResNet50 and VGG16 FR systems.

4.5 Compared with Competitive Baselines

In this section, we build two competitive baselines, permutation baseline and random baseline, to investigate whether our proprietary morphing fields can indeed be effectively served as guidance in morphing facial images. In the experiments, we mainly 1) explore the attack success rate and the intensity of morphing fields measured by ℓ_2 -norm and ℓ_∞ -norm, 2) investigate the attack success rate and the visual quality of morphed facial images with structural similarity index (SSIM) and normalized cosine similarity (NCS). Here, we consider a *region of operation* (ROO) in evaluating the performance of our proprietary morphing field compared with baselines. ROO is the region where ‘adversarial attack’ assumption holds, *i.e.*, imperceptible to human eyes.

Permutation baseline permutes the proprietary morphing fields while maintaining their intensity same as the original proprietary morphing fields. As proprietary morphing field includes horizontal channel \mathbf{f}^h and vertical channel \mathbf{f}^v , permutation baseline can permute morphing fields within channels, named *intra-channel* permutation baseline, and between two channels, named *inter-channel* permutation baseline. Random baseline randomly generated morphing field \mathbf{f}^h and \mathbf{f}^v , which follow a uniform distribution $\mathcal{U}[-2, 1]$ as more than 94.4% raw morphing fields lying in this range in the query stage. Fig. 8 presents us the experimental results of our proprietary morphing field and two baselines in attacking the VGG16 FR system. Experimental results in Fig. 8 demonstrate that our proprietary morphing field performs better than the permutation and random baseline in ROO (see the ROO divider in Fig. 8). Being able to outperform the baselines within the region of operation is what it truly matters. Fig. 8 also illustrates that the two chosen baselines also show its power in attacking FR systems. However, the two chosen baselines are considered strong baselines as they capitalize on the prior knowledge of what optical flow fields should be. It is interesting to explore some moderate baselines in our future work. Table 9 presents the experimental result in comparing with baselines where the similarity distance between original facial image and morphed facial images is measured with SSIM and NCS. It indicates that our proprietary morphing fields achieve a high attack success rate when the morphed facial images are similar to original facial images, especially the SSIM and NCS value are larger than 0.9 and 0.998, respectively. Thus, our proprietary morphing field outperforms the three random baseline when the morphed facial images appear subtle change.

5 Conclusions

In this work, we have introduced and investigated a new type of black-box adversarial attack to evade deep-learning based FR systems by morphing facial images with learned optical flows. The proposed attack morphs/deforms pixels spatially as opposed to adversarial noise attack that perturbs the pixel intensities. With a simple yet effective joint dictionary learning pipeline, we are able to obtain a

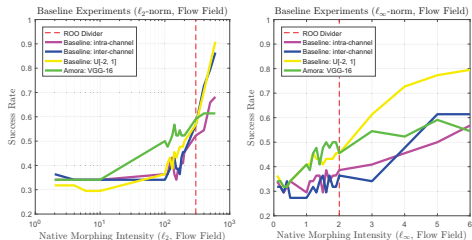


Fig. 8: Baseline experiment results on ℓ_2 -norm and ℓ_∞ -norm in attacking VGG16 FR system. Baseline: intra-channel and inter-channel are permutation baseline, Baseline: $\mathcal{U}[-2, 1]$ is random baseline. Left side of the ROO Divider is the region of operation where adversarial assumption holds. Amora trumps in the ROO.

Table 9: Attack success rate and the visual quality of morphed facial images measured with SSIM and NCS with three random baselines, $\mathcal{U}[-2, 1]$, $\mathcal{U}[-1, 1]$, and $\mathcal{N}(0, 1)$. Large SSIM and NCS values denote that the morphed facial image is similar to the original face. **Green** region is the ROO.

$\mathcal{M} \setminus \text{ssim}$	[0.75, 0.8]	[0.8, 0.85]	[0.85, 0.9]	[0.9, 0.95]	[0.95, 1.0]
VGG-16	0	0	0.048	0.073	0.373
$\mathcal{U}[-2, 1]$	0.278	0.128	0.079	0.032	0.046
$\mathcal{U}[-1, 1]$	0.346	0.181	0.104	0.073	0.035
$\mathcal{N}(0, 1)$	0.224	0.123	0.07	0.016	0.032
$\mathcal{M} \setminus \text{nCS}$	[0.990, 0.992]	[0.992, 0.994]	[0.994, 0.996]	[0.996, 0.998]	[0.998, 1.0]
VGG-16	0	0.001	0.014	0.058	0.420
$\mathcal{U}[-2, 1]$	0.032	0.091	0.185	0.355	0.222
$\mathcal{U}[-1, 1]$	0	0.006	0.046	0.279	0.444
$\mathcal{N}(0, 1)$	0.008	0.052	0.151	0.366	0.312

proprietary morphing field for each individual attack. Experimental results have shown that some popular FR systems can be evaded with high probability and the performance of these systems is significantly decreased with our attacks. Our observation has raised an essential security issue in currently deployed FR systems. Through comprehensive experiments and validations, we have shown that a black-box adversarial morphing attack is not only possible, but also compromises the FR systems significantly.

The proposed black-box adversarial morphing attack points to an orthogonal direction that can complement the existing adversarial noise attacks. Therefore, it is possible to combine various attack types in the future. Also, while presentation spoofing attacks are relatively easier to defend because they rely heavily on physical props, and adversarial noise attacks are less likely to be presented in real-world setups, it is useful to study the physical attacks based on adversarial morphing, since it is a semantically coherent attack with local facial deformation and is likely to happen in real scenarios such as an expression filter to attack mobile face authentication application (mobile payment/ social media), or in tandem with freeform optics that bends light [11], *etc.*

A Morphed facial images with proprietary morphing field

In this section, we present some high-resolution visualization of morphed facial images with learned proprietary morphing fields on ℓ_2 -norm, ℓ_∞ -norm and multiplier δ . The identity 011910 in *CelebA* is selected for showing all the morphed facial images under different intensity in our experiments. Fig. 9, Fig. 10, and Fig. 11 show the morphed facial images on ℓ_2 -norm, ℓ_∞ -norm, and multiplier δ , respectively.

A.1 Discussion

The three figures above present morphed facial images with proprietary morphing field on three different metrics with various intensities. We observed that the morphed facial images in these figures only exhibit minuscule artifacts that are imperceptible to human eyes. This is an important trait for any kosher adversarial attack, *i.e.* being imperceptible and stealthy. Our adversarial morphing attack generates more visually realistic and natural faces by perturbing pixels spatially in a coherent manner, which can potentially be applied to producing ‘deepfake’ videos to fool detectors with natural expression changed rather than perturbing pixels with additive noises.

B Morphed facial images with two baselines

In comparing the performance of our proprietary morphing field and two competitive baselines, we consider ROO where ‘adversarial attack’ assumption holds. To get an intuitive visualization of facial images morphed with our build two

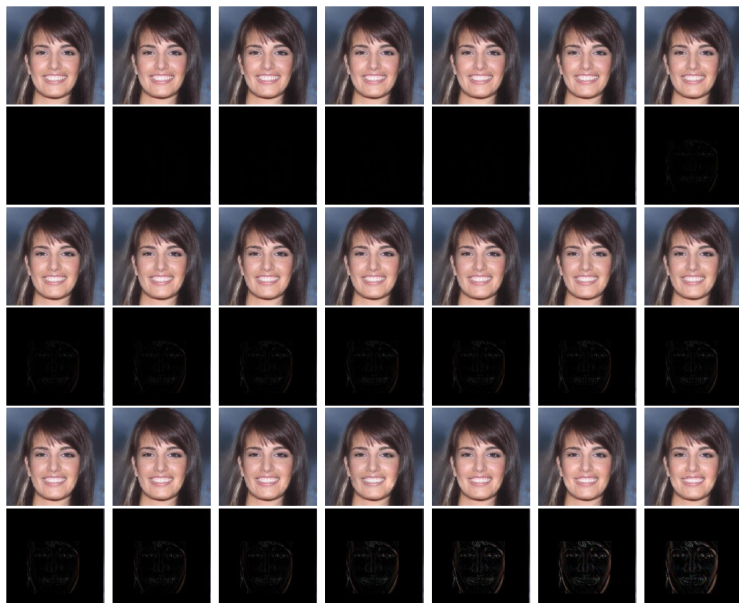


Fig.9: Original facial image (ID in *CelebA* is 011910) and morphed facial images with proprietary morphing field measured by ℓ_2 -norm. The first image is the original facial image and the next 20 images are morphed with proprietary morphing fields while images in black background are difference images of original facial image and morphed facial image. The ℓ_2 -norm values are $\{2, 4, 6, 8, 10, 100, 110, 120, 130, 140, 150, 160, 170, 180, 190, 200, 300, 400, 500, 600\}$.

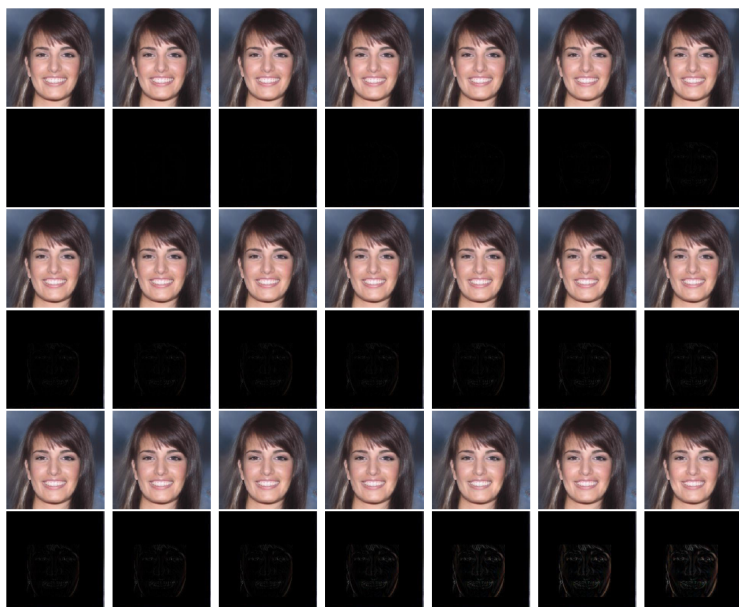


Fig.10: Original facial image (ID in *CelebA* is 011910) and morphed facial images with proprietary morphing field measured by ℓ_∞ -norm. The first image is the original facial image and the next 20 images are morphed with proprietary morphing fields while images in black background are difference images of original facial image and morphed facial image. The ℓ_∞ -norm values are $\{0.1, 0.2, 0.3, 0.4, 0.5, 1.0, 1.1, 1.2, 1.3, 1.4, 1.5, 1.6, 1.7, 1.8, 1.9, 2.0, 3.0, 4.0, 5.0, 6.0\}$.



Fig. 11: Original facial image (ID in CelebA is 011910) and morphed facial images with proprietary morphing field enhanced by multiplier δ . The first image is the original facial image and the next 10 images are morphed with proprietary morphing fields while the second row is difference images of original facial image and morphed facial image. The δ values are $\{0.2, 0.4, 0.6, 0.8, 1.0, 1.2, 1.4, 1.6, 1.8, 2.0\}$.

baselines, we present the morphed facial images with baselines in Fig. 12 on ℓ_2 -norm and ℓ_∞ -norm. The two baselines are permutation baseline (including *intra-channel* permutation baseline and *inter-channel* permutation baseline) and random baseline.

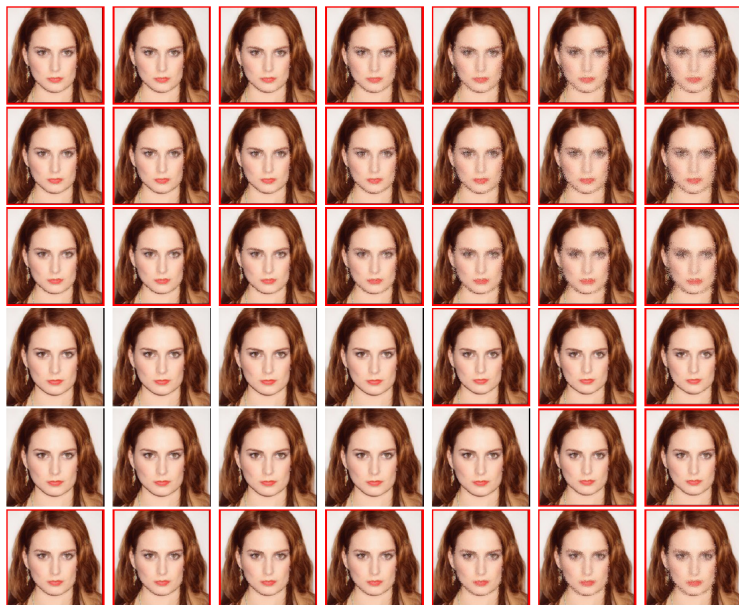


Fig. 12: Samples of morphed facial images with two competitive baselines. **The first three rows** represent the morphing fields measured by ℓ_2 -norm (values are 180, 190, 200, 300, 400, 500, 600 from the left to right) and the morphed facial images are morphed with *intra-channel* permutation baseline, *inter-channel* permutation baseline, and random baseline. **The last three rows** represent the morphing fields measured by ℓ_∞ -norm (values are 1.7, 1.8, 1.9, 2.0, 3.0, 4.0, 5.0 from the left to right) and the morphed facial images are morphed with *intra-channel* permutation baseline, *inter-channel* permutation baseline, and random baseline. Morphed facial images with **red frame** denote the image has obvious artifacts.

B.1 Discussion

The two baselines leverage prior knowledge of what optical flow fields should be and illustrate its capabilities in attacking two popular FR systems. In Figure 12, we can easily observe that the morphed facial images with two baselines show obvious artifacts when outside of the ROO. Our learned proprietary morphing fields produces perceptually realistic faces and show promising results than the two baselines within the ROO. Furthermore, the proprietary morphing field can be served as a guidance in adversarially morphing the facial images.

References

1. flownet2-pytorch: Pytorch implementation of FlowNet 2.0: Evolution of Optical Flow Estimation with Deep Networks, <https://github.com/NVIDIA/flownet2-pytorch>, (March. 2020)
2. Keras-vggface, <https://github.com/rcmalli/keras-vggface>, (March. 2020)
3. Progressive Growing of GANs for Improved Quality, Stability, and Variation, https://github.com/tkarras/progressive_growing_of_gans, (March. 2020)
4. StyleGAN Encoder - converts real images to latent space, <https://github.com/Puzer/stylegan-encoder>, (March. 2020)
5. Abdal, R., Qin, Y., Wonka, P.: Image2stylegan: How to embed images into the stylegan latent space? In: Proceedings of the IEEE International Conference on Computer Vision. pp. 4432–4441 (2019)
6. Abiantun, R., Juefei-Xu, F., Prabhu, U., Savvides, M.: SSR2: Sparse Signal Recovery for Single-Image Super-Resolution on Faces with Extreme Low Resolutions. Pattern Recognition (2019)
7. Alaifari, R., Alberti, G.S., Gauksson, T.: Adef: an iterative algorithm to construct adversarial deformations. arXiv preprint arXiv:1804.07729 (2018)
8. Biggio, B., Corona, I., Maiorca, D., Nelson, B., Šrndić, N., Laskov, P., Giacinto, G., Roli, F.: Evasion attacks against machine learning at test time. In: Joint European conference on machine learning and knowledge discovery in databases. pp. 387–402. Springer (2013)
9. BioID: BioID Face Liveness Detection. <https://www.bioid.com/liveness-detection/>, accessed: 2019-11-11
10. Bose, A.J., Aarabi, P.: Adversarial attacks on face detectors using neural net based constrained optimization. In: 2018 IEEE 20th International Workshop on Multimedia Signal Processing (MMSP). pp. 1–6. IEEE (2018)
11. Brand, M., Birch, D.A.: Freeform irradiance tailoring for light fields. Optics express **27**(12), A611–A619 (2019)
12. Carlini, N., Wagner, D.: Towards evaluating the robustness of neural networks. In: 2017 IEEE Symposium on Security and Privacy (SP). pp. 39–57. IEEE (2017)
13. Chen, P.Y., Zhang, H., Sharma, Y., Yi, J., Hsieh, C.J.: Zoo: Zeroth order optimization based black-box attacks to deep neural networks without training substitute models. In: Proceedings of the 10th ACM Workshop on Artificial Intelligence and Security. pp. 15–26. ACM (2017)
14. Deb, D., Zhang, J., Jain, A.K.: Advfaces: Adversarial face synthesis. arXiv preprint arXiv:1908.05008 (2019)
15. Dong, Y., Su, H., Wu, B., Li, Z., Liu, W., Zhang, T., Zhu, J.: Efficient decision-based black-box adversarial attacks on face recognition. In: Proceedings of the IEEE Conference on Computer Vision and Pattern Recognition. pp. 7714–7722 (2019)
16. Du, X., Xie, X., Li, Y., Ma, L., Liu, Y., Zhao, J.: Deepstellar: model-based quantitative analysis of stateful deep learning systems. In: Proceedings of the 2019 27th ACM Joint Meeting on European Software Engineering Conference and Symposium on the Foundations of Software Engineering. pp. 477–487. ACM (2019)
17. Ebrahimi, J., Rao, A., Lowd, D., Dou, D.: Hotflip: White-box adversarial examples for text classification. arXiv preprint arXiv:1712.06751 (2017)
18. Goodfellow, I., Pouget-Abadie, J., Mirza, M., Xu, B., Warde-Farley, D., Ozair, S., Courville, A., Bengio, Y.: Generative adversarial nets. In: Advances in neural information processing systems. pp. 2672–2680 (2014)

19. Goodfellow, I.J., Shlens, J., Szegedy, C.: Explaining and harnessing adversarial examples. arXiv preprint arXiv:1412.6572 (2014)
20. Grosse, K., Papernot, N., Manoharan, P., Backes, M., McDaniel, P.: Adversarial examples for malware detection. In: European Symposium on Research in Computer Security. pp. 62–79. Springer (2017)
21. Guo, Q., Juefei-Xu, F., Xie, X., Ma, L., Wang, J., Feng, W., Liu, Y.: Abba: Saliency-regularized motion-based adversarial blur attack. arXiv preprint arXiv:2002.03500 (2020)
22. Guo, Q., Xie, X., Juefei-Xu, F., Ma, L., Li, Z., Feng, W., Liu, Y.: Spark: Spatial-aware online adversarial perturbations against visual object tracking. arXiv preprint arXiv:1910.08681 (2019)
23. Huang, Y., Juefei-Xu, F., Wang, R., Xie, X., Ma, L., Li, J., Miao, W., Liu, Y., Pu, G.: FakeLocator: Robust Localization of GAN-Based Face Manipulations via Semantic Segmentation Networks with Bells and Whistles. arXiv preprint arXiv:2001.09598 (2020)
24. Ilg, E., Mayer, N., Saikia, T., Keuper, M., Dosovitskiy, A., Brox, T.: FlowNet 2.0: Evolution of optical flow estimation with deep networks. In: Proceedings of the IEEE conference on computer vision and pattern recognition. pp. 2462–2470 (2017)
25. Ilyas, A., Engstrom, L., Athalye, A., Lin, J.: Black-box adversarial attacks with limited queries and information. arXiv preprint arXiv:1804.08598 (2018)
26. Juefei-Xu, F., Pal, D.K., Savvides, M.: Hallucinating the full face from the periocular region via dimensionally weighted k-svd. In: Proceedings of the IEEE Conference on Computer Vision and Pattern Recognition Workshops. pp. 1–8 (2014)
27. Juefei-Xu, F., Pal, D.K., Savvides, M.: Nir-vis heterogeneous face recognition via cross-spectral joint dictionary learning and reconstruction. In: Proceedings of the IEEE conference on computer vision and pattern recognition workshops. pp. 141–150 (2015)
28. Juefei-Xu, F., Savvides, M.: Encoding and decoding local binary patterns for harsh face illumination normalization. In: 2015 IEEE International Conference on Image Processing (ICIP). pp. 3220–3224. IEEE (2015)
29. Juefei-Xu, F., Savvides, M.: Pokerface: partial order keeping and energy repressing method for extreme face illumination normalization. In: 2015 IEEE 7th International Conference on Biometrics Theory, Applications and Systems (BTAS). pp. 1–8. IEEE (2015)
30. Juefei-Xu, F., Savvides, M.: Fastfood dictionary learning for periocular-based full face hallucination. In: 2016 IEEE 8th International Conference on Biometrics Theory, Applications and Systems (BTAS). pp. 1–8. IEEE (2016)
31. Juefei-Xu, F., Savvides, M.: Learning to invert local binary patterns. In: BMVC (2016)
32. K, P., M, S.: Deepfakes: a new threat to face recognition? assessment and detection. arXiv:1812.08685
33. Karras, T., Aila, T., Laine, S., Lehtinen, J.: Progressive growing of gans for improved quality, stability, and variation. arXiv preprint arXiv:1710.10196 (2017)
34. Karras, T., Laine, S., Aila, T.: A style-based generator architecture for generative adversarial networks. In: Proceedings of the IEEE Conference on Computer Vision and Pattern Recognition. pp. 4401–4410 (2019)
35. Kim, J., Feldt, R., Yoo, S.: Guiding deep learning system testing using surprise adequacy. In: Proceedings of the 41st International Conference on Software Engineering. pp. 1039–1049. ICSE '19 (2019)

36. Kose, N., Dugelay, J.L.: On the vulnerability of face recognition systems to spoofing mask attacks. In: 2013 IEEE International Conference on Acoustics, Speech and Signal Processing. pp. 2357–2361. IEEE (2013)
37. Levine, A., Feizi, S.: Wasserstein smoothing: Certified robustness against wasserstein adversarial attacks. arXiv preprint arXiv:1910.10783 (2019)
38. Liu, Z., Luo, P., Wang, X., Tang, X.: Deep learning face attributes in the wild. In: Proceedings of International Conference on Computer Vision (ICCV) (December 2015)
39. Ma, L., Juefei-Xu, F., Xue, M., Li, B., Li, L., Liu, Y., Zhao, J.: Deepct: Tomographic combinatorial testing for deep learning systems. In: 2019 IEEE 26th International Conference on Software Analysis, Evolution and Reengineering (SANER). pp. 614–618. IEEE (2019)
40. Ma, L., Juefei-Xu, F., Zhang, F., Sun, J., Xue, M., Li, B., Chen, C., Su, T., Li, L., Liu, Y., et al.: Deepgauge: Multi-granularity testing criteria for deep learning systems. In: Proceedings of the 33rd ACM/IEEE International Conference on Automated Software Engineering. pp. 120–131. ACM (2018)
41. Ma, L., Zhang, F., Sun, J., Xue, M., Li, B., Juefei-Xu, F., Xie, C., Li, L., Liu, Y., Zhao, J., et al.: Deepmutation: Mutation testing of deep learning systems. In: 2018 IEEE 29th International Symposium on Software Reliability Engineering (ISSRE). pp. 100–111. IEEE (2018)
42. Madry, A., Makelov, A., Schmidt, L., Tsipras, D., Vladu, A.: Towards deep learning models resistant to adversarial attacks. arXiv preprint arXiv:1706.06083 (2017)
43. Moosavi-Dezfooli, S.M., Fawzi, A., Frossard, P.: Deepfool: a simple and accurate method to fool deep neural networks. In: Proceedings of the IEEE conference on computer vision and pattern recognition. pp. 2574–2582 (2016)
44. Narodytska, N., Kasiviswanathan, S.: Simple black-box adversarial attacks on deep neural networks. In: 2017 IEEE Conference on Computer Vision and Pattern Recognition Workshops (CVPRW). pp. 1310–1318. IEEE (2017)
45. Odena, A., Olsson, C., Andersen, D., Goodfellow, I.: TensorFuzz: Debugging neural networks with coverage-guided fuzzing. In: Chaudhuri, K., Salakhutdinov, R. (eds.) Proceedings of the 36th International Conference on Machine Learning. Proceedings of Machine Learning Research, vol. 97, pp. 4901–4911. PMLR, Long Beach, California, USA (09–15 Jun 2019)
46. Papernot, N., McDaniel, P., Goodfellow, I., Jha, S., Celik, Z.B., Swami, A.: Practical black-box attacks against machine learning. In: Proceedings of the 2017 ACM on Asia conference on computer and communications security. pp. 506–519. ACM (2017)
47. Papernot, N., McDaniel, P., Jha, S., Fredrikson, M., Celik, Z.B., Swami, A.: The limitations of deep learning in adversarial settings. In: 2016 IEEE European Symposium on Security and Privacy (EuroS&P). pp. 372–387. IEEE (2016)
48. Pei, K., Cao, Y., Yang, J., Jana, S.: Deepxplore: Automated whitebox testing of deep learning systems. In: Proceedings of the 26th Symposium on Operating Systems Principles. pp. 1–18. ACM (2017)
49. Ranjan, A., Janai, J., Geiger, A., Black, M.J.: Attacking optical flow. In: Proceedings of the IEEE International Conference on Computer Vision. pp. 2404–2413 (2019)
50. Sharif, M., Bhagavatula, S., Bauer, L., Reiter, M.K.: Accessorize to a crime: Real and stealthy attacks on state-of-the-art face recognition. In: Proceedings of the 2016 ACM SIGSAC Conference on Computer and Communications Security. pp. 1528–1540. ACM (2016)

51. Song, Q., Wu, Y., Yang, L.: Attacks on state-of-the-art face recognition using attentional adversarial attack generative network. arXiv preprint arXiv:1811.12026 (2018)
52. Wang, R., Ma, L., Juefei-Xu, F., Xie, X., Wang, J., Liu, Y.: Fakespotter: A simple baseline for spotting ai-synthesized fake faces. arXiv preprint arXiv:1909.06122 (2019)
53. Wold, S., Esbensen, K., Geladi, P.: Principal component analysis. *Chemometrics and intelligent laboratory systems* **2**(1-3), 37–52 (1987)
54. Wong, E., Schmidt, F.R., Kolter, J.Z.: Wasserstein adversarial examples via projected sinkhorn iterations. arXiv preprint arXiv:1902.07906 (2019)
55. Xiao, C., Zhu, J.Y., Li, B., He, W., Liu, M., Song, D.: Spatially transformed adversarial examples. arXiv preprint arXiv:1801.02612 (2018)
56. Xie, X., Ma, L., Juefei-Xu, F., Xue, M., Chen, H., Liu, Y., Zhao, J., Li, B., Yin, J., See, S.: Deephunter: a coverage-guided fuzz testing framework for deep neural networks. In: *Proceedings of the 28th ACM SIGSOFT International Symposium on Software Testing and Analysis*. pp. 146–157. ACM (2019)
57. Xie, X., Ma, L., Wang, H., Li, Y., Liu, Y., Li, X.: Diffchaser: Detecting disagreements for deep neural networks. In: *Proceedings of the Twenty-Eighth International Joint Conference on Artificial Intelligence, IJCAI-19*. pp. 5772–5778. International Joint Conferences on Artificial Intelligence Organization (7 2019). <https://doi.org/10.24963/ijcai.2019/800>, <https://doi.org/10.24963/ijcai.2019/800>
58. Yang, J., Wright, J., Huang, T.S., Ma, Y.: Image super-resolution via sparse representation. *IEEE transactions on image processing* **19**(11), 2861–2873 (2010)
59. Zhang, G., Yan, C., Ji, X., Zhang, T., Zhang, T., Xu, W.: Dolphinattack: Inaudible voice commands. In: *Proceedings of the 2017 ACM SIGSAC Conference on Computer and Communications Security*. pp. 103–117. ACM (2017)
60. Zhang, J., Harman, M., Ma, L., Liu, Y.: Machine learning testing: Survey, landscapes and horizons. *IEEE Transactions on Software Engineering* (2019)